



1997; O'Dowd and Smith, 1993; Quinn et al., 1998; Murphy et al., 1998; Pierce and Adams, 2006). Sea salt droplets take part in heterogeneous chemical and microphysical transformations, thus influencing trace gases in the marine boundary layer (e.g., von Glasow et al., 2002). SSA also impacts the incoming radiation. In clear sky conditions it dominates the aerosol extinction of solar radiation over larger parts of the ocean, regionally contributing more than 75% to the aerosol scattering (Haywood et al., 1999; Grini et al., 2002; Ma et al., 2008; Murphy et al., 1998). Its direct radiative effect is still highly uncertain (Lundgren et al., 2013), which is also reflected in the uncertainty in estimates of reduction of the radiation absorbed by the ocean between  $0.08\text{--}6\text{ W m}^{-2}$  (Lewis and Schwartz, 2004).

In addition to sea salt (SS), primary marine aerosol (PMA) can contain organic material (OM) (e.g., O'Dowd et al., 2004). The OM changes cloud condensation nuclei properties (Roelofs, 2008; Fuentes et al., 2010; Meskhidze et al., 2011; Westervelt et al., 2012), the direct and indirect radiative effects (Gantt et al., 2012a) and the aerosol chemistry (Smoydzin and von Glasow, 2007) compared to SS only.

Estimates of PMA distribution and effects are highly uncertain. A global source strength of  $5000\text{ Tgyr}^{-1}$  with a uncertainty factor of 4 has been reported by Lewis and Schwartz (2004). A comparison of different models showed global emission rates between 3 and  $18\text{ Tgyr}^{-1}$  (Textor et al., 2006). The high diversities in the modelled SS emission rates may be caused by insufficient process parameterisation of the emission in the currently available SS source functions. The main driver of PMA emission is the surface wind speed. While Ma et al. (2008) and Fan and Toon (2011) found no impact of the water temperature on the PMA emission fluxes, the parameterisations of Mårtensson et al. (2003), Jaeglé et al. (2011) and Sofiev et al. (2011) include the dependence on the sea surface temperature (SST). Jaeglé et al. (2011) and Sofiev et al. (2011) showed the importance of the temperature dependence for SS emission flux calculations at the global scale. At the regional scale this is indicated by the results of Tsyro et al. (2011). However, different measurements disagree in the resulting SST influence on PMA emission.

379

This study investigates the effect of SST-correction of the PMA emission flux for regional modelling. The correction functions for the PMA emission flux accounting for the SST by Jaeglé et al. (2011), Sofiev et al. (2011) and in addition a new parameterisation derived from Zábori et al. (2012) are compared with each other and with measurements from two intensive campaigns within the EMEP network in June 2006 and January 2007 as well as Berner-impactor measurements made at the Cape Verde Atmospheric Observatory at Sao Vicente in December 2007. The model simulations were carried out with the regional chemistry and aerosol transport model COSMO-MUSCAT (CONsortium of Small scale MOdelling – MUlti-Scale Chemical and Aerosol Transport model) for an “European” region including Iceland and an “African” region.

## 2 PMA emission processes

Two processes are mainly responsible for PMA emission. These are the tearing of drops from wave crests and the bursting of bubbles, which are formed by the entrainment of air to the ocean through breaking waves. The dislocation of water droplets from the wave crest occurs only at 10 m wind speeds above  $7\text{--}11\text{ ms}^{-1}$ , producing the largest sea spray particles (“spume droplets” Monahan et al., 1983) with a minimum diameter of  $40\text{ }\mu\text{m}$  and no defined maximum (Andreas, 1998). Such large droplets have high deposition and sedimentation velocities resulting in low residence times. Therefore they are less important for atmospheric microphysical and chemical processes and are usually neglected in large scale modelling.

The bubble bursting process is caused by bubbles rising back to the surface after the entrainment of air to the ocean. They emit two sorts of primary aerosols: small film droplets and larger jet droplets (Blanchard, 1963). Film droplets are formed during the collapse of a bubble from the water film, or cap of its top. During that process, up to a few hundred film droplets are produced per bubble. At 80% relative humidity these droplets have typical radii of  $r_{80} = 1\text{ }\mu\text{m}$  and less (Lewis and Schwartz, 2004). Spiel (1998) found that film droplets are emitted mainly by bigger bubbles with a bubble ra-

380



the ocean surface and allows them to thin out before bursting, which results in a shift of the particle spectra towards smaller sizes (Sellegrì et al., 2006; Modini et al., 2013).

Summarising different measurements, Gantt and Meskhidze (2013) concluded that OM can displace SS or act as additional material in the emitted aerosols. This contribution is size dependent (Gantt and Meskhidze, 2013). Due to the lack of knowledge of a detailed quantification of that effect, it was decided to treat PMA as internal mixture with SS being replaced by OM for this work. With this assumption the volume of the total emitted PMA  $V_P$  is represented by:

$$V_P = V_{SS} + V_{OM}, \quad (1)$$

where  $V_{SS}$  and  $V_{OM}$  stands for the volumes of dry SS and OM respectively. The volume ratio  $R_V$  between OM and SS is expressed as:

$$R_V = \frac{V_{OM}}{V_{SS}} \quad (2)$$

and the ratio  $R_{Vp}$  between OM and dry PMA:

$$R_{Vp} = \frac{V_{OM}}{V_P}. \quad (3)$$

### 2.3 Dependence of PMA emission on SST

The SST can influence the physical processes controlling the PMA emission flux through bubble bursting via the viscosity of the water, the surface tension at the boundary between water and air, the molecular diffusivity and the solubility of gases. These properties impact on the coalescence of the bubbles, the gas exchange between the bubble and the surrounding water and the rising speed and thus the residence time of a bubble.

The kinematic viscosity of water decreases by a factor 2.2 with a temperature change from 0 to 30°C (e.g., Chen et al., 1973). This leads to a 2.2 times lower rise speed of

383

air bubbles at 0°C due to the inverse proportional relationship assuming Stokes motion (Lewis and Schwartz, 2004). The resulting higher residence time in cold waters leads to an increase in the coalescence of bubbles, thus decreasing the number of smaller bubbles and increasing the number of bigger bubbles (Pounder, 1986).

The higher solubility of gases at cold temperatures in combination with the higher residence time of the bubbles lead to higher gas exchange rates between the bubble and the surrounding water. This is partly compensated by the lower diffusivity (Thrope et al., 1992). The gas exchange leads to a shrinking of the bubbles during their rise to the ocean surface. Smaller bubbles dissolve completely while bigger bubbles can survive. Higher exchange rates in colder waters lead to a decrease in the number of smaller bubbles resulting in a shift of the bubble size distribution towards bigger bubbles (see also Sect. 4.4.2., Fig. 35 Lewis and Schwartz, 2004).

Surface tension decreases only by 6% for temperature changes between 0 and 30°C, but may also impact the PMA emission. It may influence the breakup of bubbles in the water, bubble shape and the rising velocity as well as the breakup processes at the surface (Blanchard, 1963; Lewis and Schwartz, 2004).

In summary, lower SST lead to a decrease in the number concentration of small and an increase of large bubbles, resulting in a shift in the PMA size distribution.

Several laboratory studies confirm the influence of the SST on PMA emission (Bowyer et al., 1990; Mårtensson et al., 2003; Sellegrì et al., 2006; Hultin et al., 2011; Zábóri et al., 2012). Disagreements in the studies may be due to differences in the experimental setup. All authors found an increase in the number concentrations of small particles with decreasing temperature. Zábóri et al. (2012) found a up to 10-fold increase for particles with diameter between 0.012µm and 1.8µm when reducing temperatures from 13–16°C to 0°C. Similarly Hultin et al. (2011) and Bowyer et al. (1990) also found a 4 to 5 times increasing particle number concentration with decreasing temperature for particles with a dry diameter of 0.02µm to 1.8µm and 0.25µm to 1.5µm respectively. Finally, Mårtensson et al. (2003) also found an increase up to a size of 0.1µm in dry diameter with a continuous increase of the factor with decreasing particle





(2011) is based on the measurements of Keene et al. (2007) and Faccini et al. (2008). Keene et al. (2007) used sea water from the Bermuda Islands and Faccini et al. (2008) sampled aerosols 400 km off the Irish west coast. So in summary the salinity is approximately 35‰. To use this emission function for other salinities a corresponding particle size has to be calculated. It is assumed that the particle size is independent of salinity in the moment of the formation (RH = 98 %). With that assumption the source function defines the emission flux and the salinity the corresponding dry particle size. This will lead to a shift of the emitted particle size distributions towards smaller diameters for lower salinities, as reported by Zábory et al. (2012). No further influence of the salinity on the number production or size distribution (Mårtensson et al., 2003; Sofiev et al., 2011) has been taken into account.

The PMA emission schemes account for the fluxes at the measurement height, which is a few centimetres in case of laboratory bubble bursting experiments (Monahan et al., 1986; Bowyer et al., 1990; Mårtensson et al., 2003; Sellegri et al., 2006; Long et al., 2011) or a few meters in oceanic field studies (Smith et al., 1993; Smith and Harrison, 1998; Clarke et al., 2006). Therefore it is difficult to compare the source functions with each other because large particles quickly settle after emission. Thus the effective fluxes are calculated at a defined height. For this an equation by Hoppel et al. (2005) can be used:

$$\frac{F(z_2)}{F(z_1)} = \left(\frac{z_2}{z_1}\right)^{-\left(\frac{v_s}{\kappa u_*}\right)} \quad (11)$$

where  $F$  is the PMA flux at the heights  $z_1$  and  $z_2$ ,  $v_s$  the sedimentation velocity of the particle at 80 % relative humidity,  $\kappa$  the von Kaarman constant and  $u_*$  the friction velocity. For the height correction of surface fluxes we set  $z_1 = z_0$ , where  $z_0$  is the surface roughness length.  $z_0$  and  $u_*$  are taken from the meteorological driver model COSMO (see below). Due to the gravitational losses only particles reaching the half level height of the lowest level ( $z_{1/2}$ ) are taken into account, thus  $z_2 = z_{1/2}$  (Fan and Toon, 2011).

389

To calculate the organic mass emitted with SS few parameterisations are available, which are summarised in a comparison study by Gantt et al. (2012b). Here the parameterisation by Long et al. (2011) is used together with the assumption that OM replaces SS in the emitted aerosols. For the calculation of the volume ratio  $R_V$  of OM to dry SS (compare Eq. 2) Long et al. (2011) used the two-mode approach that was mentioned above:

For  $D_{p80} < 1 \mu\text{m}$ :

$$R_{V,1}(D_{p80}, \text{chl } a) = 0.306 \cdot D_{p80}^{\delta_1} \quad (12)$$

with

$$\delta_1 = \frac{-2.01 \cdot 40 \cdot [\text{chl } a]}{1 + 40 \cdot [\text{chl } a]} \quad (13)$$

and for  $D_{p80} > 1 \mu\text{m}$ :

$$R_{V,2}(D_{p80}, \text{chl } a) = \frac{0.056 \cdot 20.8 \cdot [\text{chl } a]}{1 + 29.8 \cdot [\text{chl } a]} \quad (14)$$

The variables  $D_{p80}$  and  $\text{chl } a$  represent the particle size at 80 % relative humidity in  $\mu\text{m}$  and the chlorophyll  $a$  concentration at the ocean surface in  $\mu\text{g L}^{-1}$ .

### 15 3.2 COSMO-MUSCAT

For this study the multi scale model system COSMO-MUSCAT (Wolke et al., 2012) is used. It was developed for process studies and operational forecast of pollutants and has been used in several air quality studies (Renner and Wolke, 2010) as well as large scale-transport studies of Saharan dust (Heinold et al., 2011). It is a online coupled system of COSMO developed by the German Weather Service (DWD) (Schättler et al., 2008) and MUSCAT (Wolke et al., 2012). The small-scale weather model COSMO is

390





southeast Norway. They are strongly influenced by marine air but located inland. Some particles can be removed before the air reaches the measurement sites. A further marine station is Virolahti II in southeast Finland, which is influenced by PMA from the low salinity Baltic Sea. The continental station Melpitz (Germany) represents long-range transport of PMA and is strongly impacted by deposition. These stations are equipped with filter pack, high- and low volume samplers and/or MARGA (Monitor for Aerosols and Gases in ambient Air) with additional chemical analysis at a height of 2 m. Mass concentrations for  $PM_1$ ,  $PM_{2.5}$  and  $PM_{10}$  are determined daily. To trace SS the sodium concentration within the observed aerosol is used, which has only minor anthropogenic sources (Tsyro et al., 2011). For the conversion from SS to sodium mass a factor of 0.3061 is used (Seinfeld and Pandis, 2006).

While the EMEP stations represent the mid latitudes with lower SST, the measurements from the Cape Verde Atmospheric Observatory (CVAO) at Sao Vicente (Table 2) represent a region with higher SST. This island lays within the Cape Verde archipelago 700 km west of Africa. Its aerosol composition is dominated by mineral dust from the Sahara, biomass burning aerosol and aerosols of marine origin (Heinold et al., 2011; Müller et al., 2010, 2011). The measurements used here were obtained with a 5-stage Berner-impactor mounted at the top of a 30 m high tower 70 m inland off the coast to avoid direct influence by sea spray. The stages of this impactor were separated into: stage 1: 0.05–0.14  $\mu\text{m}$ , stage 2: 0.14–0.45  $\mu\text{m}$ , stage 3: 0.45–1.2  $\mu\text{m}$ , stage 4: 1.2–3.5  $\mu\text{m}$ , stage 5: 3.5–10  $\mu\text{m}$  (Müller et al., 2010). The measurements used here have a daily frequency and were obtained in December 2007.

### 3.5 Description of case study and model setup

Three model simulations were carried out to capture all three measurement periods. For the comparison with the EMEP-stations in June 2006 and January 2007 an European region (Fig. 3) including the north east Atlantic as potential source for PMA was chosen. The model uses a horizontal grid resolution of  $0.25^\circ$  and 30 vertical model

393

layers in MUSCAT and 40 layers in COSMO. The mid-height of the lowest level is at approximately 10 m. The spin up time of the model is five days.

For the comparison to the measurements at Sao Vicente in December 2007 a second model domain is used (African domain) (Fig. 4). The grid resolution is the same as for the European domain except that  $z_{1/2} = 33\text{m}$ , which is close to the measurement height of the tower.

Further input data needed for the simulation of PMA emission are visualised in Figs. 3 and 4. Ocean surface salinity distribution is shown in Fig. 3 for the “European” domain. There, the yearly averaged values from the World Ocean Atlas 2001 at  $0.25^\circ$  grid resolution are taken.

The simulation of the fraction of OM within PMA requires the sea surface chlorophyll *a* concentration fields. Satellite retrievals provide the best spatial coverage. The chlorophyll product from MODIS-Aqua and MODIS-Terra were taken from the Ocean-Colour webpage. Here, the averages of the monthly mean values of both satellites were used. Missing data points were filled with the climatological monthly mean values. Remaining gaps were filled by linear interpolation (Fig. 4).

To take the influence of the SST on the PMA emission fluxes into account, SST data fields are needed. These were taken from COSMO based on the reanalysed input data of the GME model.

## 4 Model results

Since the emission flux and the vertical transport of PMA by turbulence are very sensitive to the surface wind speed it is important that the model reproduces this parameter realistically. Modelled surface wind speeds were compared to measurements made during the northward-directed Atlantic transec cruise number ANT-XXVII/4 of the research vessel *Polarstern*. The measurements of the wind speed at the *Polarstern* were made at 37 m-height, which is approximately the half level height of the lowest level of the “African” domain. The model first layer wind speeds are plotted against these

394

observations in Fig. 5. The model slightly underestimates the measured wind speeds. The slope of the regression between model and observations is 0.8 ( $R^2 = 0.68$ ). This implies that the model slightly underestimates PMA emission fluxes, due to the wind speed dependence. This would be partly compensated by an overestimated wind speed dependence in the PMA-emission flux parameterisation by Long et al. (2011). There the authors assumed all air, which is entrained into the ocean, detrains as bubbles. As mentioned above, a part of the air dissolves in the ocean during the rise back to the surface leading to a lower amount of air detraining by bubbles than entrained by wave breaking.

#### 4.1 Comparison of modelled sea salt aerosol with station data

The model results for sodium concentrations were compared with the measurements from the two EMEP-intensive campaigns in January 2007 and June 2006 (Figs. 6 and 8). The measurements (black symbols) are shown together with the model results neglecting a SST-dependence (blue lines) and using the S11-SST-correction (red lines). In all figures the EMEP-stations are sorted from north to south for January 2007 and June 2006.

To compare the model results for coarse mode particles,  $PM_{10}$ – $PM_{2.5}$  were calculated from  $PM_{10}$  and  $PM_{2.5}$  data (Fig. 6). It should be noted that the measurement uncertainties of  $PM_{10}$ – $PM_{2.5}$  thus contain the uncertainties of both measurements.  $PM_{10}$ – $PM_{2.5}$  measurement data show 2–3 times higher sodium concentrations at Auchencorth Moss, Cabauw and Melpitz in winter compared to summer. This can be attributed to the higher wintertime wind speed (Tsyro et al., 2011), which is the dominating parameter for PMA emissions. The salting of icy roads may also have an influence on the wintertime measurements, but is assumed to be of less importance (Tsyro et al., 2011). The measured sodium concentration at Virolahti is by a factor of 0.7 lower in January compared to June. This points to the importance of SST, which varies strongly in the Baltic Sea (near Virolahti) by up to a factor of 6 between January and June. At other stations it varies only by 1.8 (Irish Sea) to 3.2 (German Bay). Near Virolahti

395

the monthly averaged wind speed (model) increased by 1.8 from June to January. At Birkenes there is also a slight decrease by a factor of 0.9 in the sodium concentration, which is attributed to the different origin of the air masses in January and June. In January the main wind direction is west to northwest, resulting in a long transport time over land, which leads to a higher amount of particles to be deposited before they reach the station. In June, the main wind direction varies in such way that a higher amount of particles is advected from south to east, where transport over land is short. The highest monthly averaged sodium concentrations ( $0.69 \mu\text{g m}^{-3}$ ) are found at Cabauw in January. While the concentrations at Auchencorth Moss are clearly higher than at the inland station Melpitz with  $0.63 \mu\text{g m}^{-3}$  to  $0.4 \mu\text{g m}^{-3}$  in January, they are nearly equal in June with  $0.26 \mu\text{g m}^{-3}$  to  $0.2 \mu\text{g m}^{-3}$ . The low sodium concentration ( $0.15 \mu\text{g m}^{-3}$  in January and  $0.22 \mu\text{g m}^{-3}$  in June) at Virolahti, which is comparable to or lower than at Melpitz, results from the low salinity of the Baltic Sea impacting PMA at Virolahti. In contrast, Melpitz is influenced by air masses from the Atlantic Ocean and North Sea. The model results with the uncorrected SS source function overestimate the concentration at nearly all stations and fit only at a few points well to the measurements. The SST-correction using S11 leads to a better agreement between model results and measurements with a tendency to underestimate the measured concentration at some points, especially at peak concentrations.

The  $PM_{2.5}$  sodium concentrations in Fig. 7 show comparable features to  $PM_{10}$ – $PM_{2.5}$  with higher monthly averaged concentrations for Auchencorth Moss (3.0 times), Cabauw (1.8 times) and Melpitz (2.6 times) in winter than in summer. While the monthly average concentration at Virolahti in June is nearly equal to that in January, at Birkenes the concentration is by a factor of 3.2 lower in June compared to January, which is the highest factor for all 5 stations; and in contrast to  $PM_{10}$ – $PM_{2.5}$  where the wintertime concentration were slightly lower. This may be due to the lower deposition velocities of the smaller particles resulting in higher concentration in January, although the air mass travels a longer way over land. Once again the highest average concentration is found at Cabauw with  $1 \mu\text{g m}^{-3}$  in January and the lowest at Virolahti and Melpitz with

396



of the contribution of OM to total PMA and the use of daily resolved chlorophyll *a* concentration instead of the monthly averaged values may cause higher variability in the modelled  $R_{VP}$ . The comparison of the model results with the measurements shows that the parameterisation of Long et al. (2011) in the current setup retrieves OM volume ratios, which underestimate the measurements at the four larger impactor stages. Likely this underestimation is a result of underestimating the total OM concentration, since the sodium concentration is in good agreement with the measurements (Fig. 9). This seems to be in contrast to the results of Gantt et al. (2012b), who found the parameterisation by Long et al. (2011) overpredicts the concentration of OM at Mace Head (53.33° N, 9.90° W) and Amsterdam Island (37.80° S, 77.57° E). However, those results were compared to stations in the mid-latitudes, while here the results are compared to a station in the lower latitudes (Table 2). Also, the model assumptions differ from each other, so that the results are not directly comparable. The differing results highlight the importance of the model set up to account for the correct description of the emission rates.

### 4.3 Emission fluxes

For the two simulations in January 2007 and June 2006 the monthly averaged emission fluxes of dry submicron and supermicron PMA mass are plotted in Fig. 12. There the results without temperature correction are shown. Due to the higher wind speeds in winter especially over the Atlantic the emission rates as well as the maximum emissions are higher in January than in June, resulting in higher airborne particle concentrations. This model result reproduces the majority of the measurements (compare Figs. 6 and 7). The location of the highest emission rates differs between January and June as well. While in June the areas with the local maximal emission rates are located north west of Ireland and west of Iceland, in January the maximum emission is spread over a larger area west of Ireland and Scotland with additional strong emissions from the North Sea. The low emission rates at the Baltic Sea are due its low salinity.

399

The SST correction factors applied to the emission fluxes are recalculated from the monthly averaged total emission fluxes for submicron and for supermicron particles (Figs. 13 and 14). The factors for all size classes differ more or less strongly from each other with the majority retrieving a factor lower than 1, thus decreasing the emission rates. The emission fluxes of supermicron particles are decreased by all parameterisations. The strongest decrease was found for S11, while the highest correction factors are found for the Zb13 starting north of Great Britain, because the emissions were unaffected above  $T_W = 13^\circ\text{C}$  in that parameterisation. Apart from reducing emissions, none of the correction functions changes the regional characteristics of the emission fluxes, which remains dominated by the wind speed. J11 and S11 show the same characteristics in the submicron size fraction of PMA. The correction factor from J11 is identical for the submicron and supermicron particles, due to the missing size dependence. The submicron correction factor for S11 is higher than for supermicron particles but still below 1. This is despite the fact that the S11-SST-correction function showed an increase in the emission rates of small particles (see Fig. 1). However, since it decreases emissions for particles larger than  $0.2\mu\text{m}$  which dominate the mass of submicron particles this leads to the decrease of the total emission fluxes with temperature. Finally the Zb13-SST-correction function increases the submicron emissions for lower SST. This is because of the high factor for particles around 0.1 micron, which then dominate the size distribution. This high factor leads to changed regional characteristics of the highest PMA emission rates, which are now located at the low temperature water around Greenland. Furthermore the high correction factors at the northern Baltic Sea should be noted, which lead to strong increases in the emission rates resulting in high concentrations at Virolahti when using this function.

### 4.4 Sensivity to correction of the SST

The Figs. 15–18 show boxplots with the 5, 25, 50, 75 and 95-percentile for the measurements compared to the median of the model results, where S11 is given in red symbols, J11 in black symbols, Zb13 in green symbols and the results without SST

400

correction in blue symbols. The daily average values are used for all included data and only these model values were taken into account where measurements exist.

#### 4.4.1 $PM_{10}-PM_{2.5}$

For  $PM_{10}-PM_{2.5}$  concentrations the measurements and model results at the five EMEP-stations are plotted in Fig. 15. As explained above, the model simulates the highest sodium concentrations when using no correction for SST. All SST-correction functions lower the modelled concentrations, with Zb13 resulting in the highest and S11 the lowest values. The uncorrected values are higher than the measured ones at all stations and higher or even near the 95-percentile at the majority of the stations especially in January. For Virolahti, Birkenes and Melpitz in June the uncorrected concentrations are closer to the measured median and within the 75-percentile. The higher overprediction in January points towards the need of the SST correction. All three tested correction functions improved the model results compared to the measurements. While Zb13 and J11 lower the concentrations only a little so that there are still stations with overprediction of sodium concentrations, the S11-SST-correction function lead to underestimations of the modelled concentrations except at Auchen-corth Moss and Birkenes in January, but overall the S11-SST-correction result in the best agreement of model results and observations.

#### 4.4.2 $PM_{2.5}$

Boxplots of  $PM_{2.5}$  are shown for the same stations as for  $PM_{10}-PM_{2.5}$  (Fig. 16). In that size range no clear optimum correction function is found. The Zb13-SST-correction function increases the concentrations, because the correction factor is higher than 1 for particles smaller than  $1.8\mu\text{m}$ . This leads to worse results where the uncorrected version overpredicts the measured concentration, but improves the results at Cabauw, Auchencorth Moss in January and Melpitz in June. Since the results of the uncorrected model are close to the measurements, the S11-SST-correction function leads to strong

401

underpredictions of the measurements. Overall the J11-SST-correction function tends to result in best agreement with measurements for that case study.

#### 4.4.3 $PM_1$

It was mentioned above that the SST-correction with Zb13 retrieves high correction factors for  $PM_1$  at the northern Baltic Sea. This leads to high emission rates resulting in high modelled concentrations of marine aerosol at the station Virolahti. In Fig. 17 it can be seen that these high values lead to a strong overprediction of the sodium mass compared to the measurements, especially in January. The lower concentrations by the neglect of the SST-dependence or the use of S11 and J11 are closer to the measurements for that station. However these three model setups underpredicted the concentration at Melpitz, where the increase of the concentration by Zb13 fits best to the measurements.

#### 4.4.4 Berner-impactor at Sao Vicente

Figure 18 compares the model results with measurements of a Berner-impactor which operated at the CVAO at Sao Vicente. Due to the relatively high SST at these latitudes only a slight influence by the correction functions can be distinguished. S11 shows the strongest decrease in the concentrations, caused by the origin of the air mass, which is mainly from regions with a SST around  $20^\circ\text{C}$ . J11 does not change the concentrations compared to the uncorrected version significantly and Zb13 has no influence due to the SST being above  $13^\circ\text{C}$ .

For the second, fourth and fifth stage best agreement is for S11, but again with the tendency to underestimate the concentration. For the third stage it cannot be decided which parameterisation results in the best values in comparison with the measurements.

## 5 Discussion

The EMEP-intensive campaign measurements were also used by Tsyro et al. (2011) for the evaluation of the EMEP chemical transport model. The authors found the model to underpredict the  $PM_{2.5}$  and  $PM_{10}$  sodium concentration in June 2006 while the model underprediction is less or changes to overprediction of the measurements in January 2007. They attributed the discrepancies to inaccuracies in the wind prediction or the coarse model grid resolution ( $50\text{ km} \times 50\text{ km}$ ). The same results are found for sodium concentrations for COSMO-MUSCAT when PMA emissions are not SST corrected (Figs. 6 and 7). In contrast to the EMEP-model the sodium concentration is overestimated with the uncorrected SS source function in COSMO-MUSCAT. SST correction of the PMA emission decreases the modelled sodium concentration at the EMEP stations, so that the measurements are matched better than without correction. This is particularly evident for the  $PM_{10}$ – $PM_{2.5}$  size range and for the winter month. The strongest emission decrease was obtained by S11 resulting in underestimation of the sodium concentration at the measurement sites, while the J11-SST-correction has a smaller effect. For the coarse particles the use of the SST-correction function by S11 gives reasonable results.

The effect of the SST correction is not as clear for  $PM_{2.5}$  concentrations. For this size range the S11-SST-correction function leads to worse results compared to the other functions in the comparison with the observations. In the current work the parameterisation of Long et al. (2011) was used to describe the PMA emission flux. The use of a different PMA emission functions (e.g., Sofiev et al., 2011) (Fig. 2) with higher emission rates will result in higher non-SST-corrected  $PM_{2.5}$  sodium concentrations than with the parameterization by Long et al. (2011). In combination with the S11-SST-correction those modelled concentrations would result in better agreement with the observations at the EMEP measurement sites, but would lead to overestimations of the concentrations at Sao Vicente.

403

At Melpitz, the measured sodium concentrations in the  $PM_1$  size range decrease in January compared to June. This is in contrast to coarse particles, where they increase. This behaviour is similar for Virolahti, but less clear. Such an effect could be due to the decrease of the concentration of larger particles within the size spectrum being partly compensated by the increase of smaller particles with lower SST. However, the evaluation at only two stations and two months is insufficient to obtain statistically meaningful results. In general, the uncorrected version tends to underestimate the  $PM_1$  concentration so that the results with Zb13 are in best agreement with the measurements at the EMEP station. However, the very high correction factor for low temperatures leads to overestimations of the concentration at near coastal stations in winter as at Virolahti. Based on the small amount of available measurement data, a final conclusion for the SST-correction function regarding  $PM_1$  is not possible.

The measured sodium concentration at Virolahti is low compared to Cabauw or Auchencorth Moss, although all stations are of marine background. The reason for this is the air mass origin – Virolahti is influenced by air masses from the Baltic Sea, which has a salinity of 7‰ and lower. In contrast, the air mass arriving at Cabauw and Auchencorth Moss originates from the North Sea and the north-east Atlantic, where the salinity is around 35‰. The model captures the influence of salinity on SSA emission well.

The new SST-correction function that was based on measurements by Zábory et al. (2012) did not lead to better results compared to the other parameterizations. With that parameterization the concentrations of fine particles were overpredicted especially near cold waters, and the decrease of the coarse particle concentration was too low to reproduce the measured concentration. The size dependence of the correction factor cannot be validated by the available measurements.

The modelled monthly averaged emission fluxes of submicron primary OC for the “African” model domain in December 2007 were found to be between  $1\text{--}2\text{ ngm}^{-2}\text{ s}^{-1}$  west of Africa and the Mediterranean Sea and increase west of Europe towards

404

9 ngm<sup>-2</sup>s<sup>-1</sup> west of Great Britain. This is comparable to the multi-year average values determined by Long et al. (2011) and Spracklen et al. (2008).

## 6 Conclusions

In this work we tested the importance of considering the influence of SST on PMA emissions, together with impacts of surface winds and salinity. In particular for coarse mode particles neglecting the SST-dependence lead to overestimations of the PMA-concentrations by the model compared to measurements at land and island stations. While we find that using the correction functions by S11 and J11 improve the model performance for coarse mode particles, not enough data were available for PM<sub>1</sub> to test the role of SST in this size fraction. More measurements in this size range are required to study particle fluxes in the small sizes that are also important to study the role of PMA in cloud modification.

A size shift of the dry SSA size distribution towards smaller sizes with lower salinities could be indicated.

For the description of the contribution of OM to PMA a replacement of SS by this OM has been assumed in the combination with the Long et al. (2011) function for the description of their relation to each other. While the monthly averaged emission rates for submicron OM in December 2007 were found to be comparable to multi-year averaged values from literature, the measured ratio of OM to total PMA were underestimated at Sao Vicente. Since the used parameterization was developed from laboratory measurements it accounts only for primary OM. However secondary OM may also be part of the detected aerosols, leading to underestimations by the model results. Furthermore OM from the African continent can be detected within the measurements, which has also not been taken into account in the model. Both factors need to be discussed in future works.

*Acknowledgements.* This work was supported by the German Science Foundation (DFG) (Grant No. TG 376/6-1) and by the BMBF (Bundesministerium für Bildung und Forschung)

405

as part of the SOPRAN project (FZK 03F0611J) which is a German national contribution to the international SOLAS project.

Special thanks to the NASA for providing the chlorophyll *a* database on the OceanColor webpage and NOAA for the salinity database as part of the World Ocean Atlas 2001.

The authors thank Jan Erik Hanssen, Gerald Spindler, Timo Salmi Chiara DiMarco and the colleagues from RIVM (National Institute for Public Health and the Environment Centre for Environmental Quality) (the Netherlands) for their work on the measurement data as well as the colleagues from the Norwegian Institute for Air Research for publishing the collection of all measurement data on the EBAS webpage.

## References

- Andreas, E. L.: A new sea spray generation function for wind speeds up to 32 ms<sup>-1</sup>, *J. Phys. Oceanogr.*, 28, 2175–2184, doi:10.1175/1520-0485(1998)028<2175:ANSSGF>2.0.CO;2, 1998. 380, 387
- Barker, D. R. and Zeitlin, H.: Metal-ion concentrations in seasurface microlayer and size separated atmospheric aerosol samples in Hawaii, *J. Geophys. Res.*, 77, 5076–5086, doi:10.1029/JC077i027p05076, 1972. 382
- Blanchard, D. C.: The electrification of the atmosphere by particles from bubbles in the sea, in: *Progress in Oceanography*, vol. 1, chap. 2, Elsevier, New York, 1963. 380, 384
- Blanchard, D. C.: Sea-to-air transport of surface active material, *Science*, 146, 396–397, doi:10.1126/science.146.3642.396, 1964. 382
- Blanchard, D. C.: *The Production, Distribution, and Bacterial Enrichment of the Sea-Salt Aerosol*, D. Reidel, Dordrecht, 407–454, 1983. 381
- Bowyer, P. A., Woolf, D. K., and Monahan, E. C.: Temperature dependence of the charge and aerosol production associated with a breaking wave in a whitecap simulation tank, *J. Geophys. Res.-Oceans*, 95, 5313–5319, doi:10.1029/JC095iC04p05313, 1990. 384, 385, 389
- Carlson, D. J.: Dissolved organic materials in surface microlayers: temporal and spatial variability and relation to sea state, *Limnol. Oceanogr.*, 28, 415–431, 1983. 382
- Chen, S. F., Chan, R. C., Read, S. M., and Beomley, L. A., *Viscosity of sea water solutions, Desalination*, 13, 37–51, 1973. 383

- Clarke, A. D., Owens, S. R., and Zhou, J.: An ultrafine sea-salt flux from breaking waves: implications for cloud condensation nuclei in the remote marine atmosphere, *J. Geophys. Res.*, 111, D06202, doi:10.1029/2005JD006565, 2006. 381, 387, 389
- de Leeuw, G., Andreas, E. L., Anguelova, M. D., Fairall, C. W., Lewis, E. R., O'Dowd, C., Schulz, M., and Schwartz, S. E.: Production flux of sea spray aerosol, *Rev. Geophys.*, 49, RG2001, doi:10.1029/2010RG000349, 2011. 387
- Duce, R. A. and Hoffmann, E. J.: Chemical fractionation at the air/sea interface, *Annu. Rev. Earth Pl. Sc.*, 4, 187–228, 1976. 382
- Facchini, M. C., Rinaldi, M., Decesari, S., Carbone, C., Finessi, E., Mircea, M., Fuzzi, S., Ceburnis, D., Flanagan, R., Nilsson, E. D., de Leeuw, G., Martino, M., Woeltjen, J., and O'Dowd, C. D.: Primary submicron marine aerosol dominated by insoluble organic colloids and aggregates, *Geophys. Res. Lett.*, 35, L17814, doi:10.1029/2008GL034210, 2008. 389
- Fan, T. and Toon, O. B.: Modeling sea-salt aerosol in a coupled climate and sectional microphysical model: mass, optical depth and number concentration, *Atmos. Chem. Phys.*, 11, 4587–4610, doi:10.5194/acp-11-4587-2011, 2011. 379, 389
- Fuentes, E., Coe, H., Green, D., de Leeuw, G., and McFiggans, G.: On the impacts of phytoplankton-derived organic matter on the properties of the primary marine aerosol – Part 1: Source fluxes, *Atmos. Chem. Phys.*, 10, 9295–9317, doi:10.5194/acp-10-9295-2010, 2010. 379, 382
- Gantt, B. and Meskhidze, N.: The physical and chemical characteristics of marine primary organic aerosol: a review, *Atmos. Chem. Phys.*, 13, 3979–3996, doi:10.5194/acp-13-3979-2013, 2013. 382, 383, 392
- Gantt, B., Meskhidze, N., Facchini, M. C., Rinaldi, M., Ceburnis, D., and O'Dowd, C. D.: Wind speed dependent size-resolved parameterization for the organic mass fraction of sea spray aerosol, *Atmos. Chem. Phys.*, 11, 8777–8790, doi:10.5194/acp-11-8777-2011, 2011. 382, 398
- Gantt, B., Xu, J., Meskhidze, N., Zhang, Y., Nenes, A., Ghan, S. J., Liu, X., Easter, R., and Zaveri, R.: Global distribution and climate forcing of marine organic aerosol – Part 2: Effects on cloud properties and radiative forcing, *Atmos. Chem. Phys.*, 12, 6555–6563, doi:10.5194/acp-12-6555-2012, 2012a. 379, 382
- Gantt, B., Johnson, M. S., Meskhidze, N., Sciare, J., Ovadnevaite, J., Ceburnis, D., and O'Dowd, C. D.: Model evaluation of marine primary organic aerosol emission schemes, *Atmos. Chem. Phys.*, 12, 8553–8566, doi:10.5194/acp-12-8553-2012, 2012b. 382, 390, 399

- Gong, S. L.: A parameterization of sea-salt aerosol source function for sub- and super-micron particles, *Global Biogeochem. Cy.*, 17, 1097, doi:10.1029/2003GB002079, 2003. 381, 387, 388
- Grini, A., Myhre, G., Sundet, J. K., and Isaksen, I. S. A.: Modeling the annual cycle of sea salt in the Global 3-D Model Oslo CTM2, concentrations, fluxes and radiative impact, *J. Climate*, 15, 1717–1730, doi:10.1175/1520-0442(2002)015<1717:MTACOS>2.0.CO;2, 2002. 379
- Hardy, J. T.: The sea surface microlayer: biology, chemistry and antropogenic emrnichment, *Prog. Oceanogr.*, 11, 307–328, 1982. 382
- Haywood, J. M., Ramaswamy, V., and Soden, B. J.: Tropospheric aerosol climate forcing in clear-sky satellite observations over the oceans, *Science*, 283, 1299–1303, doi:10.1126/science.283.5406.1299, 1999. 379
- Heinold, B., Tegen, I., Bauer, S., and Wendisch, M.: Regional modelling of Saharan dust and biomass-burning smoke, *Tellus B*, 63, 800–813, doi:10.1111/j.1600-0889.2011.00574.x, 2011. 390, 393
- Hoffman, E. J. and Duce, R.: Organic carbon in marine atmospheric particulate matter: concentration and particle size distribution, *Geophys. Res. Lett.*, 4, 449–452, doi:10.1029/GL004i010p00449, 1977. 382
- Hoppel, W. A., Caffrey, P. F., and Frick, G. M.: Particle deposition on water: surface source versus upwind source, *J. Geophys. Res.*, 110, D10206, doi:10.1029/2004JD005148, 2005. 389
- Hultin, K. A. H., Krejci, R., Pinhassi, J., Gomez-Consarnau, L., Mårtensson, E. M., Hagström, Å., and Nilsson, E. D.: Aerosol and bacterial emissions from Baltic seawater, *Atmos. Res.*, 99, 1–14, doi:10.1016/j.atmosres.2010.08.018, 2011. 384, 385
- Jaeglé, L., Quinn, P. K., Bates, T. S., Alexander, B., and Lin, J.-T.: Global distribution of sea salt aerosols: new constraints from in situ and remote sensing observations, *Atmos. Chem. Phys.*, 11, 3137–3157, doi:10.5194/acp-11-3137-2011, 2011. 378, 379, 380, 385
- Keene, W. C., Maring, H., Kieber, D. J., Maben, J. R., Pszenny, A. A. P., Dahl, E. E., Izaguirre, M. A., Davis, A. J., Long, M. S., Zhou, X., Smoydzin, L., von Glasow, R., and Sander, R.: Chemical and physical characteristics of nascent aerosols produced by bursting bubbles at a model air–sea interface, *J. Geophys. Res.*, 112, D21202, doi:10.1029/2007JD008464, 2007. 381, 389, 392



- Lewis, E. R. and Schwartz, S. E.: Sea Salt Aerosol Production: Mechanisms, Methods, Measurements and Models: a Critical Review, American Geophysical Union, Washington D.C., 2004. 379, 380, 381, 382, 384
- Lewis, E. R. and Schwartz, S. E.: Comment on “size distribution of sea-salt emissions as a function of relative humidity?”, *Atmos. Environ.*, 40, 588–590, doi:10.1016/j.atmosenv.2005.08.043, 2006. 392
- Long, M. S., Keene, W. C., Kieber, D. J., Erickson, D. J., and Maring, H.: A sea-state based source function for size- and composition-resolved marine aerosol production, *Atmos. Chem. Phys.*, 11, 1203–1216, doi:10.5194/acp-11-1203-2011, 2011. 382, 387, 388, 389, 390, 391, 395, 399, 403, 405
- Lundgren, K., Vogel, B., Vogel, H., and Kottmeier, C.: Direct radiative effects of sea salt for the Mediterranean region under conditions of low to moderate wind speeds, *J. Geophys. Res. Atmos.*, 118, 1906–1923, doi:10.1029/2012JD018629, 2013. 379, 387
- Ma, X., von Salzen, K., and Li, J.: Modelling sea salt aerosol and its direct and indirect effects on climate, *Atmos. Chem. Phys.*, 8, 1311–1327, doi:10.5194/acp-8-1311-2008, 2008. 379
- Mårtensson, E. M., Nilsson, E. D., de Leeuw, G., Cohen, L. H., and Hansson, H.-C.: Laboratory simulations and parameterization of the primary marine aerosol production, *J. Geophys. Res.*, 108, 4297, doi:10.1029/2002JD002263, 2003. 379, 381, 384, 385, 386, 387, 389
- Maria, S. F., Russell, L. M., Gilles, M. K., and Myneni, S. C. B.: Organic aerosol growth mechanisms and their climate-forcing implications, *Science*, 306, 1921–1924, doi:10.1126/Science.1103491, 2004. 392
- Meskhidze, N., Xu, J., Gantt, B., Zhang, Y., Nenes, A., Ghan, S. J., Liu, X., Easter, R., and Zaveri, R.: Global distribution and climate forcing of marine organic aerosol: 1. Model improvements and evaluation, *Atmos. Chem. Phys.*, 11, 11689–11705, doi:10.5194/acp-11-11689-2011, 2011. 379, 382
- Modini, R. L., Russel, L. M., Deane, G. B., and Stokes, M. D.: Effect of soluble surfactant on bubble-produced aerosol particles, *J. Geophys. Res.-Atmos.*, 118, 1288–1400, doi:10.1002/jgrd.50186, 2013. 383
- Monahan, E. C. and O’Muircheartaigh, I.: Optimal power-law description of oceanic whitecap coverage dependence on wind speed, *J. Phys. Oceanogr.*, 10, 2094–2099, 1980. 381
- Monahan, E. C., Fairall, C. W., Davidson, K. L., and Boyle, P. J.: Observed inter-relations between 10 m winds, ocean whitecaps and marine aerosols, *Q. J. Roy. Meteor. Soc.*, 109, 379–392, 1983. 380

- Monahan, E. C., Spiel, D. E., and Davidson, K. L.: A model of marine aerosol generation and wave disruption, in: *Oceanic Whitecaps and Their Role in Air–Sea Exchange Processes*, edited by: Monahan, E. C. and MacNoicaill, G., Springer, New York, 167–174, 1986. 381, 387, 389, 392
- Müller, K., Lehmann, S., van Pinxteren, D., Gnauk, T., Niedermeier, N., Wiedensohler, A., and Herrmann, H.: Particle characterization at the Cape Verde atmospheric observatory during the 2007 RHAMBLE intensive, *Atmos. Chem. Phys.*, 10, 2709–2721, doi:10.5194/acp-10-2709-2010, 2010. 393, 397, 398
- Müller, T., Schladitz, A., Kandler, K., and Wiedensohler, A.: Spectral particle absorption coefficients, single scattering albedos and imaginary parts of refractive indices from ground based in situ measurements at Cape Verde Island during SAMUM-2, *Tellus B*, 63, 573–588, doi:10.1111/j.1600-0889.2011.00572.x, 2011. 393
- Murphy, D. M., Anderson, J. R., Quinn, P. K., McInnes, L. M., Brechtel, F. J., Kreidenweis, S. M., Middlebrook, A. M., Posfai, M., Thomson, D. S., and Buseck, P. R.: Influence of sea-salt on aerosol radiative properties in the Southern Ocean marine boundary layer, *Nature*, 392, 6265, doi:10.1038/32138, 1998. 379
- Nilsson, E. D., Rannik, Ü., Swietlicki, E., Leck, C., Aalto, P. P., Zhou, J., and Norman, M.: Turbulent aerosol fluxes over the Arctic Ocean: 2. Winddriven sources from the sea, *J. Geophys. Res.*, 106, 32111–32124, doi:10.1029/2000JD900747, 2001. 381
- Oceancolor: available at: <http://oceancolor.gsfc.nasa.gov/>, last access: 13 June 2012.
- O’Dowd, C. D. and de Leeuw, G.: Marine aerosol production: a review of the current knowledge, *Philos. T. Roy. Soc.*, 365, 1753–1774, doi:10.1098/rsta.2007.2043, 2007. 378
- O’Dowd, C. D. and Smith, M. H.: Physicochemical properties of aerosols over the northeast Atlantic: evidence for wind-speed-related submicron sea-salt aerosol production, *J. Geophys. Res.*, 98, 1137–1149, doi:10.1029/92JD02302, 1993. 379, 381
- O’Dowd, C. D., Facchini, M. C., Cavalli, F., Ceburnis, D., Mircea, M., Decesari, S., Fuzzi, S., Yoon, Y. J., and Putaud, J.-P.: Biogenically driven organic contribution to marine aerosol, *Nature*, 431, 676–680, doi:10.1038/nature02959, 2004. 379, 382
- Oppo, C., Bellandi, S., Degli Innocenti, N., Stortini, A. M., Loglio, G., Schiavuta, E., and Cini, R.: Surfactant components of marine organic matter as agents for biogeochemical fractionation and pollutant transport via marine aerosols, *Mar. Chem.*, 63, 235–253, doi:10.1016/S0304-4203(98)00065-6, 1999. 382

- Pierce, J. R. and Adams, P. J.: Global evaluation of CCN formation by direct emission of sea salt and growth of ultrafine sea salt, *J. Geophys. Res.*, 111, D06203, doi:10.1029/2005JD006186, 2006. 379
- Polarstern on [www.awi.de](http://www.awi.de): available at: [http://www.awi.de/en/infrastructure/ships/polarstern/meteorological\\_observatory/continuous\\_measurements/sensor\\_information/](http://www.awi.de/en/infrastructure/ships/polarstern/meteorological_observatory/continuous_measurements/sensor_information/), last access: 13 August 2013.
- Pounder, C. D.: Sodium chloride and water temperature effects on bubbles, in: *Oceanic Whitecaps and Their Role in Air–Sea Exchange Processes*, edited by: Monahan, E. C. and Mac Nicaill, G., D. Reidel, Norwell, Mass., 278–279, 1986. 384
- Pruppacher, H. R. and Klett, J. D.: *Microphysics of Clouds and Precipitation*, Kluwer Academic Publishers, Dordrecht, 1997. 378
- Quinn, P. K., Coffman, D. J., Kapustin, V. N., Bates, T. S., and Covert, D. S.: Aerosol optical properties in the marine boundary layer during the first Aerosol Characterization Experiment (ACE 1) and the underlying chemical and physical aerosol properties, *J. Geophys. Res.*, 103, 16547–16563, doi:10.1029/97JD02345, 1998. 379
- Renner, E. and Wolke, R.: Modelling the formation and atmospheric transport of secondary inorganic aerosols with special attention to regions with high ammonia emissions, *Atmos. Environ.*, 44, 1904–1912, doi:10.1016/j.atmosenv.2010.02.018, 2010. 390
- Rinaldi, M., Facchini, M. C., Decesari, S., Carbone, C., Finessi, E., Mircea, M., Fuzzi, S., Ceburnis, D., Ehn, M., Kulmala, M., de Leeuw, G., and O’Dowd, C. D.: On the representativeness of coastal aerosol studies to open ocean studies: Mace Head – a case study, *Atmos. Chem. Phys.*, 9, 9635–9646, doi:10.5194/acp-9-9635-2009, 2009. 382
- Roelofs, G. J.: A GCM study of organic matter in marine aerosol and its potential contribution to cloud drop activation, *Atmos. Chem. Phys.*, 8, 709–719, doi:10.5194/acp-8-709-2008, 2008. 379, 382
- Russell, L. M., Hawkins, L. N., Frossard, A. A., Quinn, P. K., and Bates, T. S.: Carbohydrate-like composition submicron atmospheric particles and their production from ocean bubble bursting, *P. Natl. Acad. Sci. USA*, 107, 6652–6657, doi:10.1073/pnas.0908905107, 2010. 382
- Schättler, U., Doms, G., and Schraff, C.: A Description of the Nonhydrostatic Regional COSMO-Model, Deutscher Wetterdienst, Offenbach, available at: <http://www.cosmo-model.org>, 2008. 390

- Schulz, M., de Leeuw, G., and Balkanski, Y.: Sea-salt aerosol source functions and emissions, in: *Emissions of Atmospheric Trace Compounds*, edited by: Granier, C., Artaxo, P., and Reeves, C., Kluwer, Dordrecht, the Netherlands, 333–359, 2004. 387
- Sciare, J., Favez, O., Sarda-Estève, R., Oikonomou, K., Cachier, H., and Kazan, V.: Long-term observations of carbonaceous aerosols in the Austral Ocean atmosphere: evidence of a biogenic marine organic source, *J. Geophys. Res.*, 114, D15302, doi:10.1029/2009JD011998, 2009. 382
- Seinfeld, J. H. and Pandis, S. N.: *Atmospheric Chemistry and Physics – from Air Pollution to Climate Change*, 2nd Edn., John Wiley and Sons, New York, 2006. 391, 393
- Sellegri, K., O’Dowd, C. D., Yoon, Y. J., Jennings, S. G., and de Leeuw, G.: Surfactants and submicron sea spray generation, *J. Geophys. Res.*, 111, D22215, doi:10.1029/2005JD006658, 2006. 382, 383, 384, 387, 389
- Smith, M. H. and Harrison, N. M.: The sea spray generation function, *J. Aerosol Sci.*, 29, Supplement 1, S189–S190, doi:10.1016/S0021-8502(98)00280-8, 1998. 381, 389
- Smith, M. H., Park, P. M., and Consterdine, I. E.: Marine aerosol concentrations and estimated fluxes over the sea, *Q. J. Roy. Meteor. Soc.*, 119, 809–824, doi:10.1002/qj.49711951211, 1993. 381, 387, 389
- Smoydzin, L. and von Glasow, R.: Do organic surface films on sea salt aerosols influence atmospheric chemistry? – a model study, *Atmos. Chem. Phys.*, 7, 5555–5567, doi:10.5194/acp-7-5555-2007, 2007. 379
- Spiel, D. E.: On the birth of film drops from bubbles bursting on seawater surfaces, *J. Geophys. Res.*, 95, 18281–18288, 1998. 380
- Spracklen, D. V., Arnold, S. R., Carslaw, K. S., Sciare, J., and Pio, C.: Globally significant oceanic source of organic carbon aerosol, *Geophys. Res. Lett.*, 35, L12811, doi:10.1029/2008GL033359, 2008. 405
- Sofiev, M., Soares, J., Prank, M., de Leeuw, G., and Kukkonen, J.: A regional-to-global model of emission and transport of sea salt particles in the atmosphere, *J. Geophys. Res.*, 116, D21302, doi:10.1029/2010JD014713, 2011. 378, 379, 380, 385, 386, 387, 389, 403, 415
- Textor, C., Schulz, M., Guibert, S., Kinne, S., Balkanski, Y., Bauer, S., Bernsten, T., Berglen, T., Boucher, O., Chin, M., Dentener, F., Diehl, T., Easter, R., Feichter, H., Fillmore, D., Ghan, S., Ginoux, P., Gong, S., Grini, A., Hendricks, J., Horowitz, L., Huang, P., Isaksen, I., Iversen, I., Kloster, S., Koch, D., Kirkevåg, A., Kristjansson, J. E., Krol, M., Lauer, A., Lamarque, J. F., Liu, X., Montanaro, V., Myhre, G., Penner, J., Pitari, G., Reddy, S., Seland, Ø., Stier, P.,

- Takemura, T., and Tie, X.: Analysis and quantification of the diversities of aerosol life cycles within AeroCom, *Atmos. Chem. Phys.*, 6, 1777–1813, doi:10.5194/acp-6-1777-2006, 2006. 379
- Thrope, S. A., Bowyer, P., and Woolf, D. K.: Some factors affecting the size distributions of oceanic bubbles, *J. Phys. Oceanogr.*, 22, 382–289, doi:10.1175/1520-0485(1992)022<0382:SFATSD>2.0.CO;2, 1992. 384
- Tsyro, S. and Erdman, L.: Parameterization of Aerosol Deposition Processes in EMEP MSC-E and MSC-W Transport Models, EMEP/MSC-E & MCS-WNote 7/00, Norwegian Meteorological Institute, Oslo, 2000. 391
- 10 Tsyro, S., Aas, W., Soares, J., Sofiev, M., Berge, H., and Spindler, G.: Modelling of sea salt concentrations over Europe: key uncertainties and comparison with observations, *Atmos. Chem. Phys.*, 11, 10367–10388, doi:10.5194/acp-11-10367-2011, 2011. 379, 392, 393, 395, 403
- 15 Turpin, B. J., Saxena, P., and Andrews, E.: Measuring and simulating particulate organics in the atmosphere: problems and prospects, *Atmos. Environ.*, 34, 2983–3013, doi:10.1016/S1352-2310(99)00501-4, 2000. 398
- von Glasow, R., Sander, R., Bott, A., and Crutzen, P. J.: Modeling halogen chemistry in the marine boundary layer, 1. Cloudfree MBL, *J. Geophys. Res.*, 107, 4341, doi:10.1029/2001JD000942, 2002. 379
- 20 Westervelt, D. M., Moore, R. H., Nenes, A., and Adams, P. J.: Effect of primary organic sea spray emissions on cloud condensation nuclei concentrations, *Atmos. Chem. Phys.*, 12, 89–101, doi:10.5194/acp-12-89-2012, 2012. 379, 382
- Wolke, R., Schröder, W., Schrödner, R., and Renner, E.: Influence of grid resolution and meteorological forcing on simulated European air quality: a sensitivity study with the modeling system COSMO-MUSCAT, *Atmos. Environ.*, 53, 110–130, doi:10.1016/j.atmosenv.2012.02.085, 2012. 390, 391
- 25 World Ocean Atlas 2001: available at: [www.nodc.noaa.gov/OC5/WOA01/qd\\_ts01.html](http://www.nodc.noaa.gov/OC5/WOA01/qd_ts01.html), last access: 4 May 2011.
- Wu, J.: Oceanic whitecaps and sea state, *J. Phys. Oceanogr.*, 9, 1064–1068, doi:10.1175/1520-0485(1979)009<1064:OWASS>2.0.CO;2, 1979. 382
- 30 Yttri, K.-E., Aas, W., Tørseth, K., Stebel, K., Nyíri, Á., Tsyro, S., Merckova, K., Wankmüller R., Winiwarter, W., Bauer, H., Caseiro, A., Puxbaum, H., Holzer-Popp, T., and Schroedter-

- Homscheidt, M.: Transboundary particulate matter in Europe, Status report 2008, Joint CCC & MSC-W & CEIP report 2008, Oslo, 2008. 392
- Zábori, J., Matisáns, M., Krejci, R., Nilsson, E. D., and Ström, J.: Artificial primary marine aerosol production: a laboratory study with varying water temperature, salinity, and succinic acid concentration, *Atmos. Chem. Phys.*, 12, 10709–10724, doi:10.5194/acp-12-10709-2012, 2012. 380, 384, 385, 386, 387, 389, 404
- 5

**Table 1.** Parameters for Eq. (5) by Sofiev et al. (2011).

Temperature/°C	<i>a</i>	<i>b</i>
-2	0.092	-0.96
5	0.15	-0.88
15	0.48	-0.36
25	1	0

**Table 2.** Geographical position of the stations used for model evaluation.

Station	Country	Latitude	Longitude
Virolahti II	Finland	60.527° N	27.686° E
Birkenes	Norway	58.383° N	8.25° E
Auchencorth Moss	Great Britain	55.793° N	3.245° W
Cabauw	Netherlands	51.97° N	4.93° E
Melpitz	Germany	51.53° N	12.93° E
Sao Vincente	Cape Verde	16.864° N	24.417° W

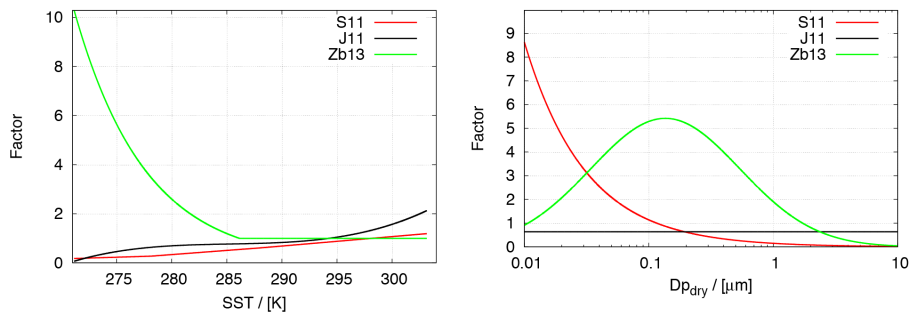


**Fig. 1.** Temperature dependence and size distribution of three functions for the SST correction factor for particles with a dry particle diameter  $D_p = 500$  nm (left) and for a SST of  $5^\circ\text{C}$  (right).

417

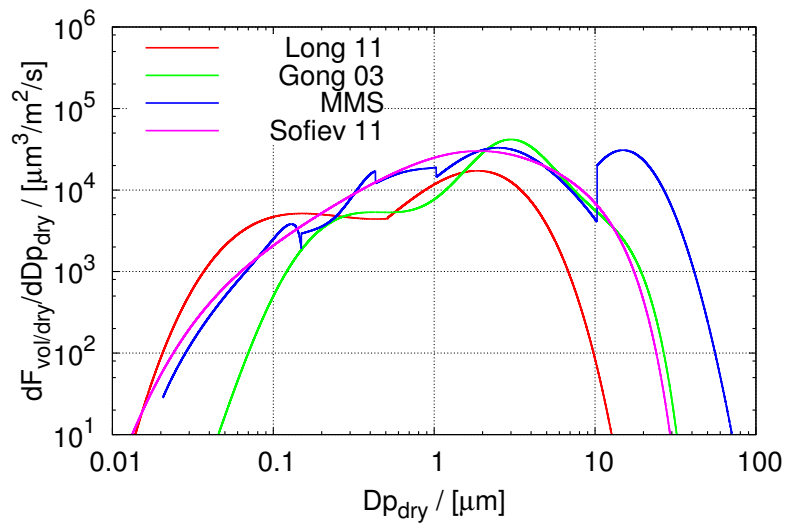


**Fig. 2.** Effective PMA volume emission flux at 10 m height for 4 sea salt source functions for dry SSA at a 10 m-wind speed of  $U_{10} = 10 \text{ m s}^{-1}$ , a salinity of  $s = 35\text{‰}$  and a SST of  $T_w = 25^\circ\text{C}$ .

418

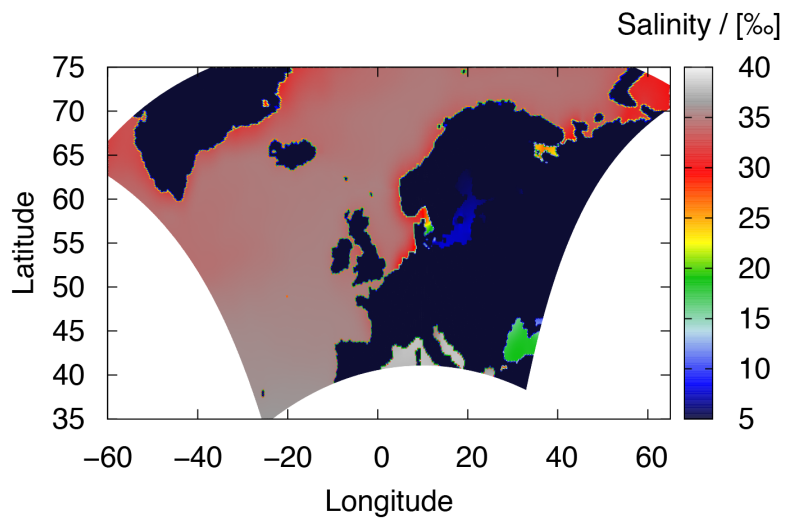


**Fig. 3.** Yearly averaged surface salinity data from World Ocean Atlas 2001.

419

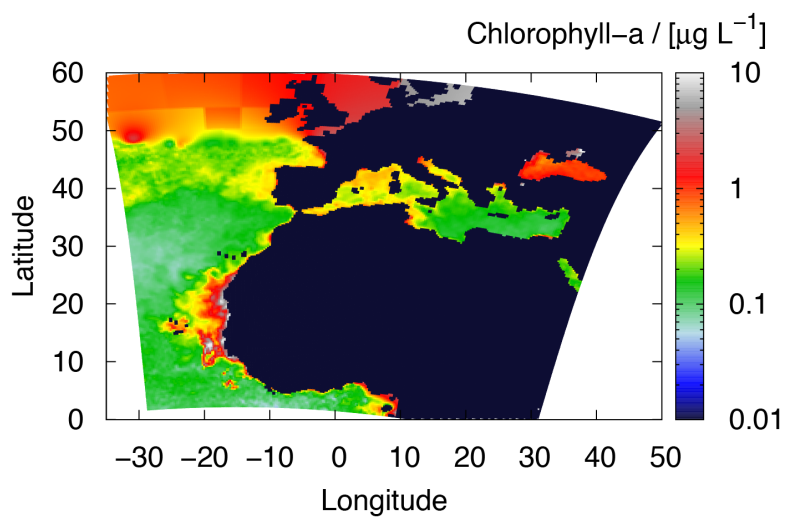


**Fig. 4.** Monthly averaged surface chlorophyll *a* concentration merged and interpolated from MODIS-AQUA and MODIS-TERRA data for December 2007.

420

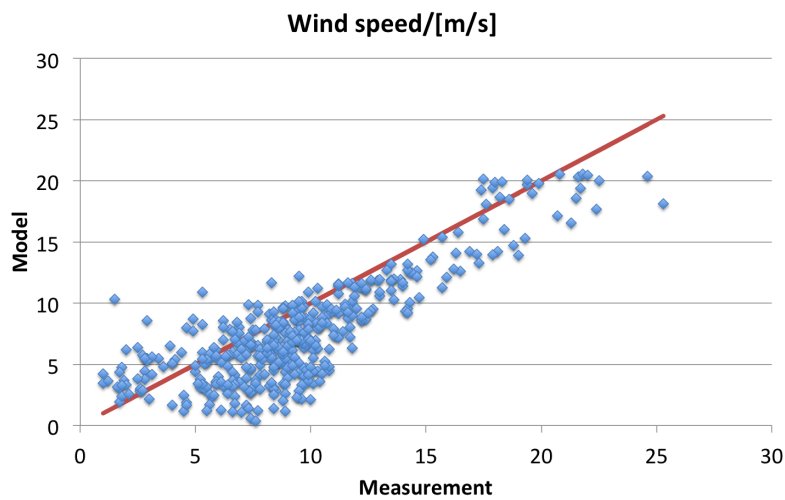


**Fig. 5.** Modelled first layer wind speed compared to measurements made during an Atlantic transect (Cape Town towards Bremerhaven) with the research vessel *Polarstern* between 28 April 2011 and 17 May 2011 compared to the 1 : 1 line.

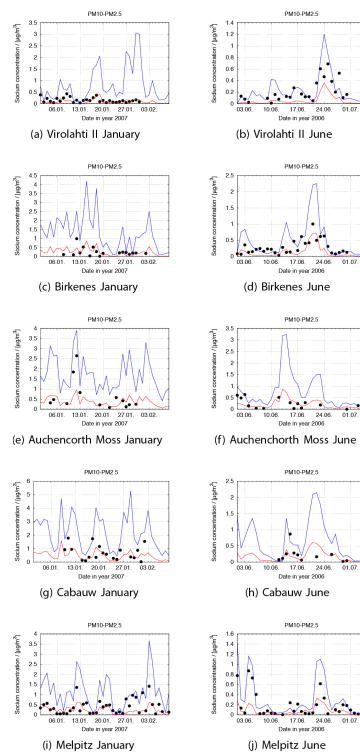


**Fig. 6.** Modelled  $PM_{10}-PM_{2.5}$  sodium mass concentration without SST correction (blue lines) and with SST correction using S11 (red lines) compared to EMEP measurements (black symbols).

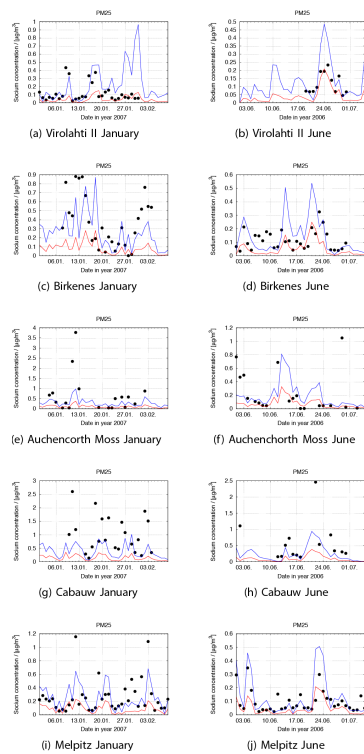


**Fig. 7.** Modelled  $PM_{2.5}$  sodium mass concentration without SST correction (blue lines) and with SST correction using S11 (red lines) compared to EMEP measurements (black symbols).

423

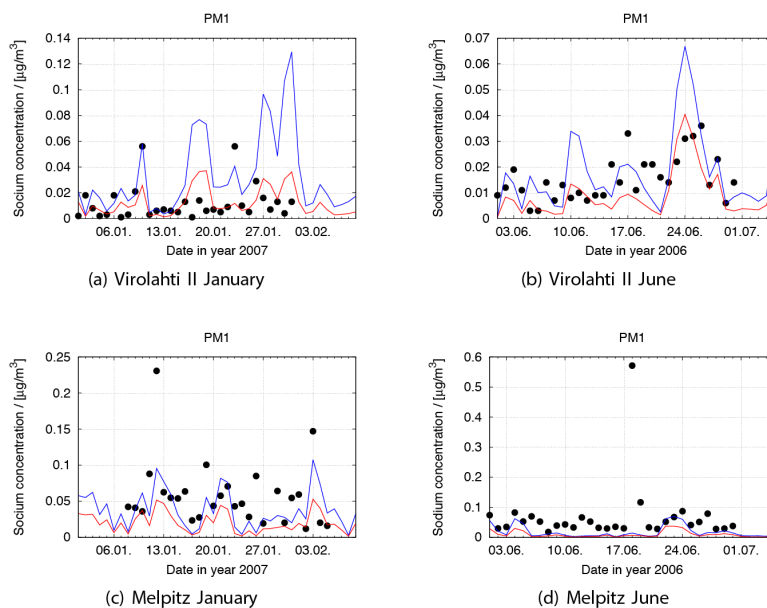


**Fig. 8.** Modelled  $PM_1$  sodium mass concentration without SST correction (blue lines) and with SST correction using S11 (red lines) compared to EMEP measurements (black symbols).

424



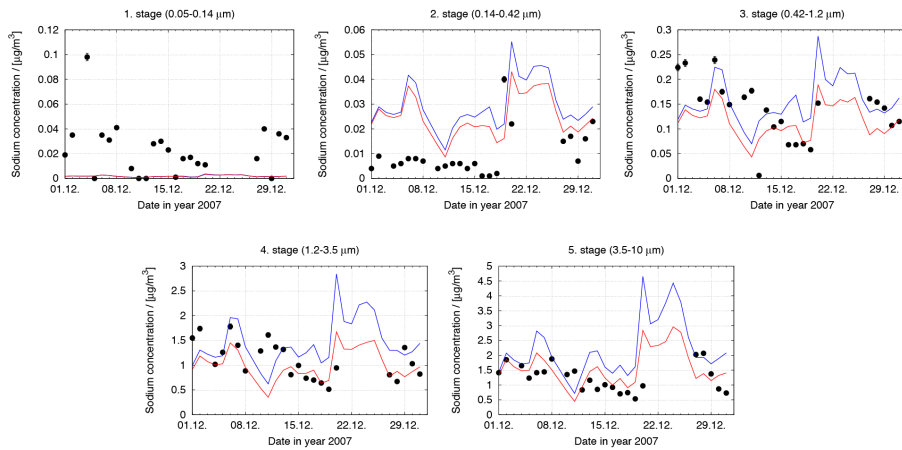


**Fig. 9.** Modelled sodium mass concentration without SST correction (blue lines) and with SST correction using S11 (red lines) compared to the Berner-impactor measurements at Sao Vincente (black symbols) for December 2007.

425

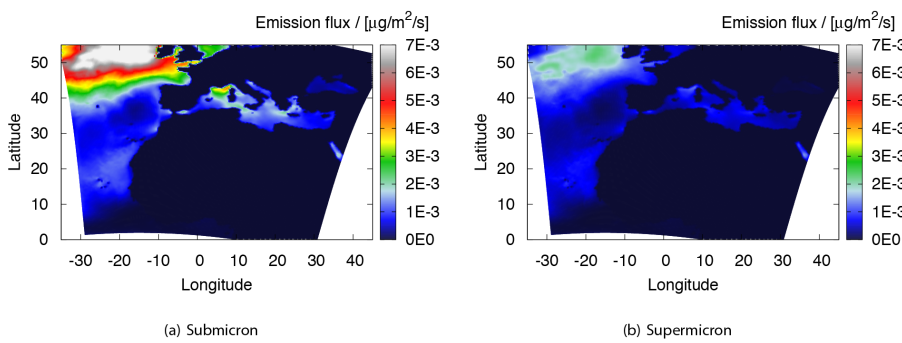


**Fig. 10.** Modelled monthly averaged emission fluxes of organic carbon for December 2007.

426

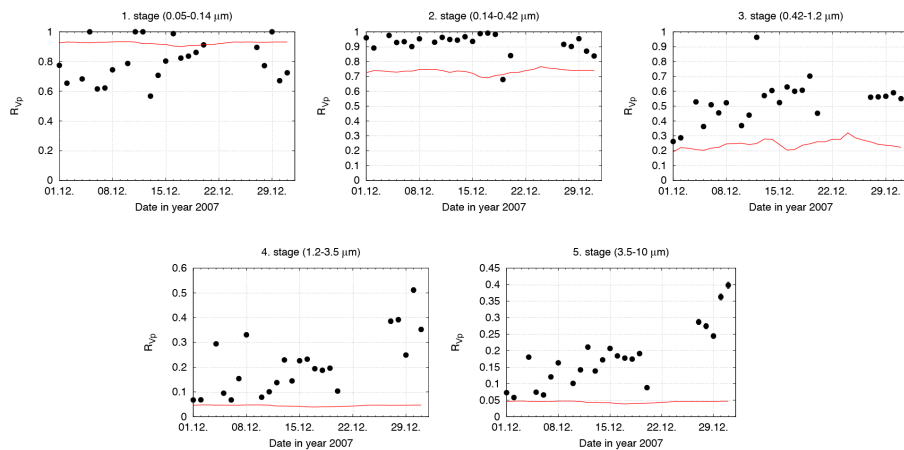


**Fig. 11.** Modelled  $R_{Vp} = V_{OM}/V_p$  in the aerosol phase compared to measurements with a Berner-impactor at Sao Vicente (Cape Verde).

427

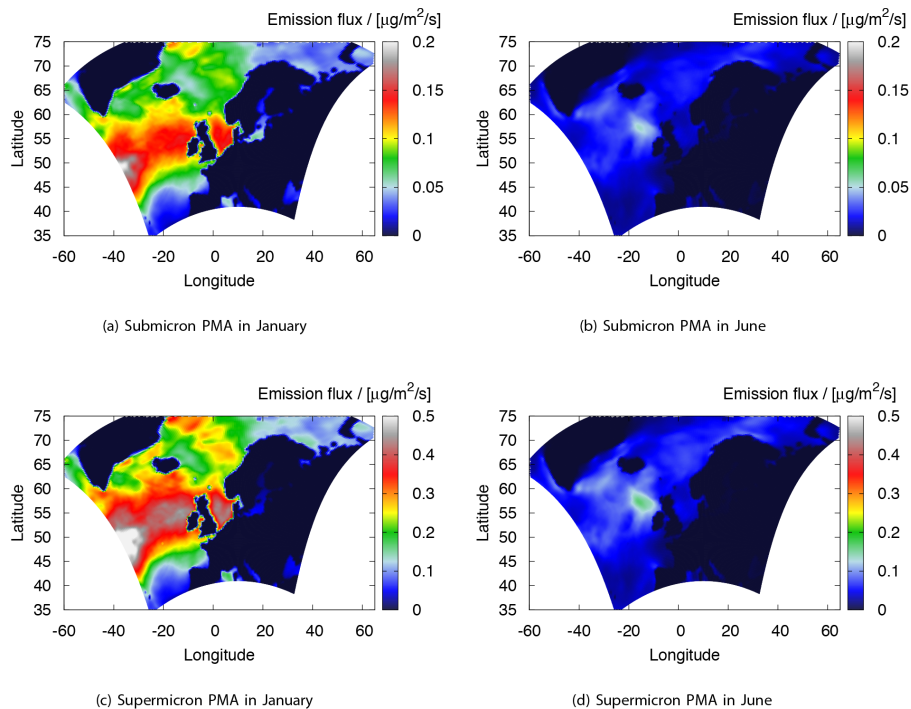


**Fig. 12.** Monthly averaged total PMA mass emission fluxes for submicron (top panels) and super micron (bottom panels) PMA emission in January 2007 (left panels) and June 2006 (right panels).

428

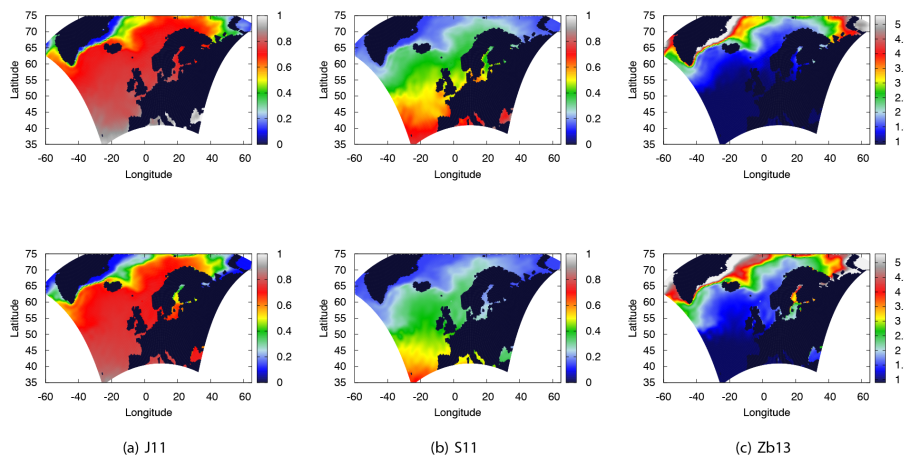


**Fig. 13.** Monthly averaged SST-correction factors for submicron PMA emission in June 2006 (top panels) and January 2007 (bottom panels) for the different parameterizations.

429

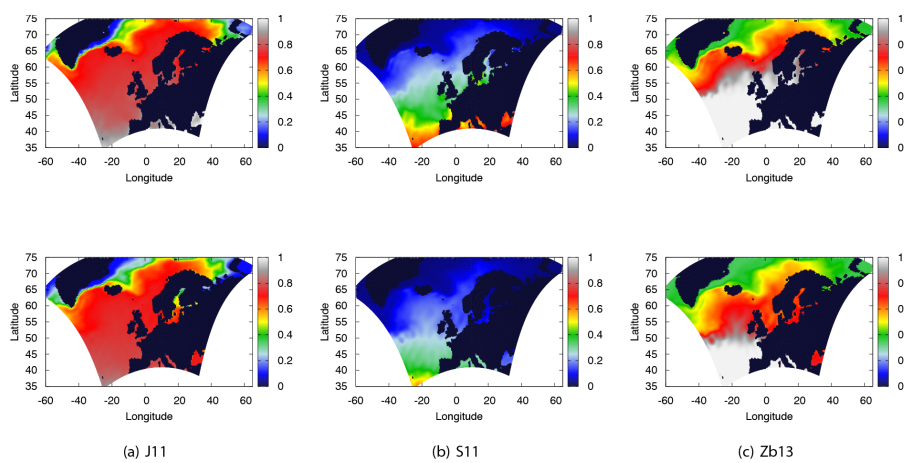


**Fig. 14.** Monthly averaged SST-correction factors for supermicron PMA emission in June 2006 (top panels) and January 2007 (bottom panels) for the different parameterizations.

430

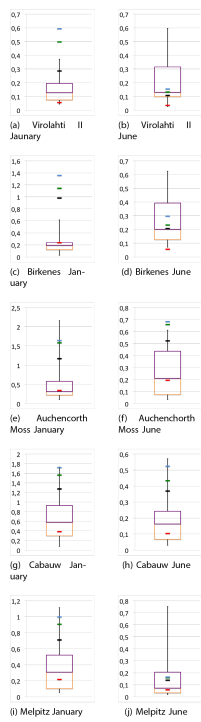


**Fig. 15.** Median of the sodium mass concentration in  $PM_{10}-PM_{2.5}$  in  $\mu g m^{-3}$  for S11 (red symbol), J11 (black symbol), Zb13 (green symbol) and no SST correction (blue symbol) compared to EMEP measurements.

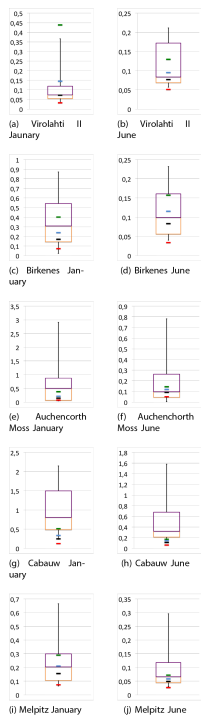


**Fig. 16.** Median of the sodium mass concentration in  $PM_{2.5}$  in  $\mu g m^{-3}$  for S11 (red symbol), J11 (black symbol), Zb13 (green symbol) and no SST correction (blue symbol) compared to EMEP measurements.

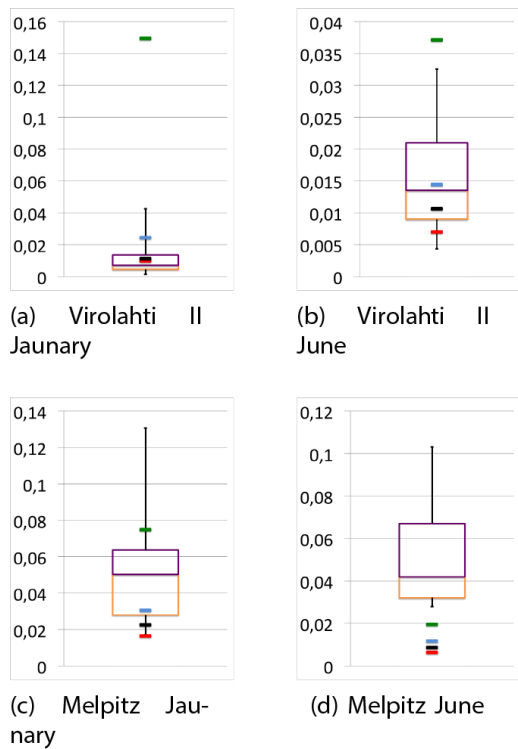


**Fig. 17.** Median of the sodium mass concentration in  $PM_1$  in  $\mu g m^{-3}$  for S11 (red symbol), J11 (black symbol), Zb13 (green symbol) and no SST correction (blue symbol) compared to EMEP measurements.

433

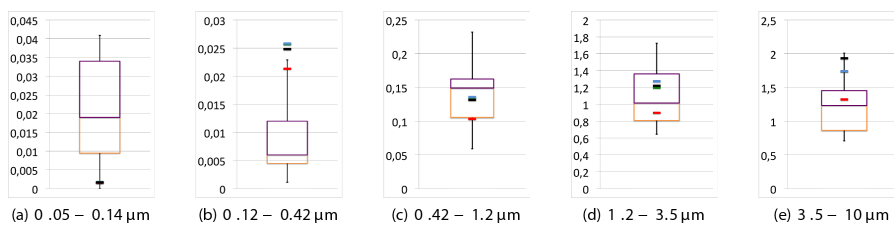


**Fig. 18.** Sodium mass concentration in  $\mu g m^{-3}$  for S11 (red symbol), J11 (black symbol), Zb13 (green symbol) and no SST correction (blue symbol) compared to Berner-impactor measurements (Boxplot) at Sao Vicente.

434